Sustainable Development in Dye Waste Management: A Comparative Study on the Effectiveness of Adsorption and γ-Radiolysis

Anupama Prabhala[1,2*], Naina Raje[3], Sanjay Sethi[2],Sangita Pal[1,4], Beena G Singh[1,5]

[1]Homi Bhabha National Institute, Anushakti Nagar, Mumbai - 400094

[2]Advanced Tuneable Laser Applications Division, BARC, Mumbai

[3]Analytical Chemistry Division, BARC, Mumbai

[4]Board of Research in Nuclear Sciences, DAE, Mumbai

[5]Radiation & Photochemistry Division, BARC (Bhabha Atomic Research Centre), Mumbai, India - 400085

Email: [*]anuvivek@barc.gov.in

Received: 13.3.2024, Revised: 5.4.2024, 14.4.2024, Accepted: 15.4.24

ABSTRACT

Pyrromethene 567 (PM567), a BODIPY class of dye; is widely used in medicine, chemistry, material science, and high-power dye lasers. During its use, PM567 dye waste is generated in ethanol solvent which needs to be treated before its disposal. In our study, we aim to compare the effectiveness of two methods for PM567 liquid waste treatment: γ-radiolysis, an advanced oxidation process (AOP), and adsorption, a simple and easy option. Interestingly, we observed that AOPs like γ-radiolysis were not efficient for dye effluent treatment in organic solvents. This inefficiency was attributed to competing reactions leading to the scavenging of dye-degrading radicals. At the highest γ-dose rate (3.5 kGy) feasible in the system; 62% is the maximum removal efficiency achieved by this method. For a comparison, we also investigated the adsorption efficiency of PM567 dye from ethanol solvent using commercially available adsorbents. Among these, powdered activated carbon (PAC) demonstrated the highest removal efficiency, reaching 95%, much higher than that of γ-radiolysis method. In line with the pursuit of sustainable development, we synthesized granular activated carbons (AC1, AC2, AC3) from coconut shells, a lignocellulosic bio-waste. The characterization of these carbons revealed that AC3, with a higher iodine value and CCl_4 activity, possessed a systematic pore structure (SEM analysis), a larger specific surface area (1708 $m^2.g^{-1}$), and a higher micro-pore volume (0.61 $cc.g^{-1}$). AC3 hence, emerged as the most effective adsorbent, achieving 95% efficiency comparable to PAC.

These findings highlight the significant potential of AC3 for liquid dye waste treatment, emphasizing its role in addressing environmental challenges and contributing to the promotion of sustainable development.

Keywords: Adsorption, Advanced oxidation processes (AOPs), BODIPY dye, Activated carbon, ethanol solvent, waste treatment

Introduction

The BODIPY class of dyes stand out as a versatile group with applications spanning diverse fields, from medicine to material sciences. These dyes, including Pyrromethene 567 (PM567), have proven invaluable in drug delivery, fluorescent probes, switches, electroluminescent films, solar cell sensitizers, and more, owing to their exceptional physicochemical properties[1]. However, industrial processes utilizing BODIPY fluorescent dyes, such as PM567 in high-power liquid dye lasers, face challenges due to photochemical degradation during operation, leading to decreased laser efficiency and hence a need for periodic dye solution replacement arises[2, 3, 4]. This replacement generates liquid waste containing dye in ethanol solvent, a concern also prevalent in industries using alcohol dyeing. The disposal of this liquid waste is typically managed through incineration [5, 6].

In response to the environmental impact of dye effluent treatment, different studies have pioneered an eco-friendly approach for treating the dye effluent, prioritizing sustainable methods over conventional practices. The literature available reveals a number of aqueous dye effluent treatment methods, which include physical separation, chemical treatment, advanced oxidation processes (AOPs), adsorption and biological methods [7]. AOPs, specifically gamma radiolysis, have demonstrated effectiveness in degrading aqueous dye effluent by utilizing ionizing radiation to generate oxidizing and reducing agents derived from radiolysis of the solvent[8].

Adsorption known for its simplicity, and versatility in treating various effluent streams, emerges as another important method. Adsorbents such as silica gel, alumina, mesoporous carbon microbeads (MCMB), powdered activated carbon (PAC), Poly (2-hydroxyethyl methacrylate), (PHEMA) and Polymethyl methacrylate (PMMA) resin, have been found to be effective adsorbents for dyes due to their large surface area and pore volume[9, 10, 11, 12, 13]. The commercially available adsorbents are however costly because of their synthetic origin [14]. Moreover, natural waste-derived activated carbons (ACs) have gained attention due to their cost effectiveness and environmental sustainability[15].

A comparative analysis between γ-radiolysis and adsorption, assessing their efficacy as dye treatment methods for PM567 in ethanol is carried out in this study. Also, motivated by the abundant availability of coconut shells, a bio-waste product available in tropical countries like India, this study focuses on synthesizing ACs from coconut shell[16]. The comparative performance evaluation for PM567 dye adsorption in ethanol by the coconut shell-derived ACs with that of the most efficient commercial adsorbent is carried out. Furthermore, through these investigations, a step has been taken towards the development of sustainable and effective solutions for treatment of liquid waste containing dye in non-aqueous systems like ethanol.

Experimental

Chemicals and reagents

PM567 was synthesized at BARC and ethanol of > 99% purity was purchased from Advent Chembio, India respectively. The properties of PM567 are given in Table 1. Silica gel, alumina, PHEMA, PMMA resins and PAC (M/s. Merck make) were procured from M/s. VRS Enterprises, Mumbai, India. Mesocarbon microbeads (MCMB) of carbon were supplied by M/s. Nanoshel, India. In this study, ACs (AC1, AC2 and AC3) were prepared by physical method in which carbonization was followed by steam activation.

Instrumental techniques

The γ-radiolysis was carried out using a GC-5000 (M/s. BRIT make) γ- irradiator with ^{60}Co source with capacity of 14,000 Ci and maximum dose rate of ~ 4.4 kGy/hr as measured by Fricke dosimetry[17]. Pulsed radiolysis coupled with absorption detection was carried out using LINAC Facility (7 MeV, 2 μs) available at RPCD, BARC [18]. Absorption spectra were recorded on a UV-visible spectrophotometer (Lab India -UV-3000+) in an optical quartz cell of 10 mm path-length at 25 ºC for all the experiments. IR spectra were recorded using diamond single reflectance ATR in MIRacle™ ATR spectrometer. The samples were analysed over the range of 400–4000 $cm^{-1}$with a 4 cm^{-1} resolution. Netzsch thermo-balance (Model No.: STA 409 PC Luxx) was used for the TG-DTA studies. For the TGA studies, Pt vs. Pt-10% Rh thermocouple was used as a temperature sensor. Simultaneous TG–DTA data analysis was done using Proteus software from Netzsch. In the TG-DTA analysis, accurately weighed AC samples (5 to 10 mg quantity) were taken and heated in air/inert atmosphere in re-crystallized alumina crucibles from room temperature to 1000 ºC at a heating rate of 10ºC min^{-1}. High purity nitrogen flow was maintained at 100 mL min^{-1} for transport of the volatile

products. SEM images were generated by an electron microscope using an SEM of SEC Co. Ltd., South Korea. The surface area of the ACs was obtained using Brunauer–Emmer–Teller (BET) method with nitrogen adsorption at − 196 °C. Analysis was conducted using a Thermo Fisher Scientific S.p.A (model: SURFER ANALYZER) nitrogen adsorption–desorption analyser and the associated software. AC of ~ 0.5 g was taken and vacuum degassed at 250 °C overnight to remove any previously adsorbed vapours from the adsorbent. The sample cell was cooled to liquid N_2 temperature to obtain detectable amounts of N_2 gas adsorption. The N_2 gas was then fed in to the sample cell, maintained under partial vacuum condition and a number of data points were collected using highly accurate pressure transducers until saturation pressure was reached. After the adsorption cycle, the desorption cycle of the sample was obtained by heating the sample and recording the data.

γ-radiolysis of PM567

The γ-radiolysis experiments of PM567 dye in ethanol were carried out in batch mode. The PM567 dye solution of a fixed feed concentration, (C_0, 200 μM) was radiolysed with a Co-60 γ-source. The radiolysis was carried out in the dose range of 0.25 kGy to 3.5 kGy. The initial concentration of the dye, C_0 and the concentration C_D, after radiolysis at a particular dose were measured by UV-absorption spectrometry. An absorption spectrum was recorded in the wave-length range 300 – 600 nm, the peak absorption was found to be at 518 nm (extinction coefficient of 65170$M^{-1}cm^{-1}$ in ethanol, Fig. 1). The G value, the radiation chemical yield, (i.e., the number of moles of PM567 dye degraded.J^{-1} of absorbed energy) is a measure of the degradation efficiency. G-value of the dye degraded in ethanol was estimated by equation (1).

$$G = \frac{(C_0 - C_D) * 0.789}{D * 10^6} \quad (1)$$

Where, C_0 and C_D are the molar dye concentrations (μM) initially and after gamma radiolysis at a given dose, D is dose in Gy and 0.789 is the ethanol density in kg.$litre^{-1}$ at room temperature.

Activated carbon synthesis

The process of activating coconut shell consists of two-steps, i.e., carbonization and activation. In the first step of carbonization, the raw and cleaned ligno-cellulosic coconut shell is thermally treated to increase the carbon composition in the shell[19]. This is done by heating the shells in underground covered pits at around 500ºC. After the carbonization the

material was cooled to room temperature and crushed. Further, the crushed charcoal was activated by physical steam activation method[19]. For this, the crushed shells along with saturated steam were fed into a rotary kiln. The temperature in the reaction zone was around 800ºC. The contact time in the central reaction zone of the carbon material varied approximately from 20min, 40 min and 120 min for the three different activated carbons AC1, AC2 and AC3 respectively. The air-cooled product was removed after the required contact time, washed, dried, sieved and tested for physico-chemical properties before adsorption studies. A BSS mesh size of 60/30 mesh (250 - 500 μm) range was chosen for all the three prepared ACs.

Physico-chemical characterization

The physico-chemical properties of the prepared ACs i.e., the bulk density, moisture content, ash content, hardness, pH, CCl_4 value (IS 877: 1989) and Iodine number (IS 2752: 1995) were estimated and the procedure has been discussed in brief[20, 21]. The apparent bulk density of ACs was calculated by recording the tapped volume occupied by 40 g of AC in a 100 mL graduated cylinder. For estimating the hardness of the ACs, a pre-weighed sample of AC was contacted with 12.7 mm and 9.5 mm diameter steel balls in a sieve shaker (15 numbers each) for 30 minutes. The sample was then sieved using 600-micron IS sieve. The weight of carbon retained above the mesh as a percentage of the total initial weight is the ball-pan hardness of the given AC. The moisture percentage of the AC was calculated from the weight loss of the pre-weighed activated carbon after heating at 110 ºC ± 5 ºC for 4 h in an oven and subsequently cooling it in a desiccator. Similarly, the ash content was obtained from the percentage weight loss in the initial weight on heating in a muffle furnace for 1000 ºC ± 5 ºC for 4 h. The carbon tetrachloride (CCl_4) activity of AC was estimated by passing CCl_4 gas over dried AC taken in an adsorption tube and measuring the final steady weight gained due to its adsorption as a percentage of the initial carbon weight. AC was dried, ground to pass through 75 micron IS sieve and then weighed accurately. The iodine number (IV) was estimated by treating 0.2 g of this dried AC with 40 mL of freshly prepared 0.1 N iodine solution for 4 minutes. The iodine solution after contacting with the AC was filtered and 10 mL of the filtrate was titrated against standard sodium thiosulphate solution. The iodine number is reported as iodine adsorbed per g of the dried AC (mg. g^{-1}).The zeta (ζ) potential of the three ACs was measured in water using Zetasizer instrument, M/s. Malvern Panalytical after sonicating the AC samples for 15 min.

Comparative batch adsorption study

All the batch studies were carried out in a M/s. Scigenic Biotech, OrbitechLTmodel, orbital shaker equipped with temperature controller incubator system. For comparing adsorption efficiency of the different ACs and commercial adsorbents, 20 mL of 200 µM PM567 prepared in ethanol was treated with a fixed amount of adsorbents (0.115g). The contact time was 4 h. The speed of orbital shaker and temperature was 150 ± 3 rpm and 25 ± 0.5 ºC, respectively. After 4 h of contact, the clear supernatant was analysed for PM567 concentration by monitoring the absorbance at 518 nm. The adsorption efficiency (%) was calculated by following equation (2), where $C_0$is the initial dye concentration, C_t is the dye concentration at time t (4 h), post adsorption.

$$\text{Adsorption efficiency } \% = \frac{(C_0 - C_t)\ \text{x}100}{C_0} \qquad (2)$$

Results & Discussion

γ-radiolysis of PM567:

Radiolysis of deaerated ethanol by γ- photon leads to the generation of primary species, namely the hydroxyethyl radical ($R^{\bullet}$), solvated electron, (e^-_{sol}), and solvent radical cation ($CH_3CH_2OH^{\bullet+}$)[22]. However, during spur expansion, the predominant radicals are $R^{\bullet}$ and e^-_{sol}. These radicals exhibit reducing properties, and in the presence of oxygen they undergo a reaction to produce peroxyl radical, which possesses oxidising characteristics. The G-value, representing the yield of $R^{\bullet}$ and the peroxyl radical, is estimated to be 0.31 µmol.J^- [122]. Assuming the initial concentration of oxygen in the aerated ethanol is 1 mM, and from the reported G-value of the $R^{\bullet}$ and the peroxyl radical, it is reasonable to expect the presence of oxygen until the absorbed dose of 3.5 kGy. As peroxyl radicals are known to have higher degradation ability and to avoid the cost of usage of inert gas like nitrogen and argon, the study was restricted mainly under aerated condition and in the absorbed dose range of 0.25 kGy to 3.5 kGy.

The effect of γ- irradiation on the degradation of PM567 in ethanol at different absorbed doses (Figure 2), shows that the dye concentration decreased from 195 µM to 158 µM (19%) at an absorbed dose of 0.25 kGy and from 195 µM to 77 µM (60.5%) at 3.3 kGy. Even on further increasing the dose to 3.5 kGy the dye degradation increase was only marginal (1.5%) (Figure 3). Additionally, the temperature of the dye solution in ethanol increased by nearly 10 ^{0}C while irradiating over the entire dose range of 0.25 kGy to 3.5

kGy. This led to ethanol vaporization, which condensed into the dye solution in the bottle after natural cooling outside the gamma chamber at the end of experiment (Figure 4). The experiment was not carried out at higher absorbed doses (max. 3.5 kGy) due to the vaporization of ethanol, potentially leading to a safety hazard and also due to the flattening of the degradation efficiency at 3.3 kGy. The average G-value of the degraded dye was estimated by plotting the decrease in concentration as a function of the absorbed dose (Figure 5). The resulting graph was linear and the slope equated to the average ($G\text{-}_{PM567}$) value (dye degraded /joule of energy) which was estimated to be 21nmol.J^{-1}. This value is lower by orders of magnitude than that observed in aqueous medium[23]. The presence of an intercept value of 29.6 µmol/l (Figure 5) indicates the presence of competing reactions like geminate recombination of the primary radicals produced during oxidation of PM567 by peroxyl radicals. Such reactions are prevalent in the organic solvent with lower dielectric constant which results in lower $G_{\text{-PM567}}$ as compared to aqueous solution. Further, the reaction between the radicals produced by radiolysis of ethanol with PM567 in real time scale was studied by employing pulse radiolysis studies using a LINAC[24]. The transient absorption spectra produced during the oxidation of PM567 by peroxyl radical under ambient air saturated condition showed formation of transient absorption maxima at 340 nm, 430 nm and 580 nm (Figure 6a). In analogy to the transient spectrum obtained from photolysis experiments, these species have been attributed to the formation of BODIPY radical cation formed by initially charge separated species[25]. The degradation of PM567 on oxidation is expected to be initiated by radical cation formation followed by ring opening [26]. The radiolysis under argon saturated condition, which is expected to remove oxygen and form a reducing species, generated transient absorption spectrum with maximum at 550 nm (Figure 6b). In analogy to previous report, this species was attributed to formation of BODIPY radical anion [27]. Unlike in aqueous medium, the lower G-value of the radical derived from ethanol reduces the dye degradation efficiency. It could thus be concluded that direct radiolysis of ethanolic dye solutions is not very effective in dye degradation.

Comparison of Adsorption efficiency of commercial adsorbents:

The comparison of adsorption of PM567 dye in ethanol for the various chosen commercial adsorbents after 4 h (contact time) is presented in Figure 7. PHEMA, MCMB had a very low efficiency of around 2%. Alumina and PMMA had 6% and silica gel 26%. The highest adsorption efficiency was observed with PAC at 95%. It is possible that lower specific surface area of MCMB, PHEMA, PMMA and alumina resulted in low dye adsorption

efficiency[28, 11]. The PAC in its powdered form was likely to have high adsorption efficiency due to the high specific surface area. It was thus concluded that among the adsorbents tested, PAC was the most efficient adsorbent. In general, for scale-up of adsorption process, packed adsorber columns are employed. The very small particle size of PAC ($\leq$ 0.18 mm ϕ) makes it difficult to use in a packed adsorption column due to a high pressure drop[29]. However, as granular AC adsorbent ($\geq$ 0.2 mm ϕ) is suitable for packed beds, synthesis of granular activated carbon from coconut shell, a biowaste was taken up.

Characterization of synthesized activated carbons:

The coconut shell (CS) mainly consists of C, O, H as elemental constituents which in turn constitute the principle lignocellulosic polymers of cellulose, hemicellulose and lignin[30]. The composition of the three fractions in a carbon source mainly depend on the particular species, age, weather and the season when the product is reaped[19]. The cellulose and hemicellulose are reported to typically contain around 65% in the CS, while lignin is found to be slightly less than 30% in composition[31].

The CS is generally carbonized using kiln or pit methods to convert them into carbon. The carbonization was carried out at 500^0C by the pit method as it is less energy intensive. The temperature chosen was above 600^0C; as a decrease in the yield of the char was reported above this temperature[19]. Carbonization resulted in the formation of carbon, after the moisture, volatiles, followed by aromatics of low molecular weight and hydrogen gas were evolved resulting in a fixed carbon skeleton filled with tar-like products. Further activation was required to produce AC with the required surface and textural properties. The AC from CS could be prepared by either physical or chemical activation process. In the chemical activation method, alkaline and acidic reagents like NaOH, KOH, $ZnCl_2$, and H_3PO_4 induce porosity in the carbon[32]. But chemical methods have their own intrinsic limitations as they generate additional chemical waste. In this work, the carbonized CS was physically activated in a rotary kiln using steam by an optimized method to prepare AC having higher surface area. The rotation of the kiln improved the heat transfer and provided good contact between the carbon particles and the steam. The water gas evolved due to the reaction between carbon and steam in the kiln led to the activation of the carbon[33].

The evidence of successful carbonization and activation was confirmed by monitoring the surface functional groups before carbonization and after activation by using FTIR (Figure 8). Non-carbonized coconut shell-based material showed stretching at 3350 cm^{-1}, 2920 cm^{-1},

1728 cm^{-1}, 1240 cm^{-1} and 1031 cm^{-1}. The bands at 3350 cm^{-1} and 2920 cm^{-1} corresponds to O-H and C-H stretching vibration, respectively. The bands at 1728 cm^{-1}, 1240 cm^{-1} and 1031 cm^{-1} correspond to vibrations due to carbonyl group, which was due to C=O stretching, C-O stretching in aromatic ester and C-O stretching respectively. A band of weak intensity in the region 1680-1620 cm^{-1} corresponds to aromatic C=C stretching. The FTIR spectrum of AC was devoid of the aforementioned functional group except that the peaks at 1735 cm^{-1}, 1370 cm^{-1} and 1220 cm^{-1}, which can be attributed to respective –C=O, O-H stretching in phenol and C-O stretching vibration from carbonyl group confirming the removal of non-carbon component and complete carbonization[34].

The physico-chemical properties of ACs tabulated in Table 2 show that most of the properties like the bulk density, moisture content, ash content (%) and hardness were not significantly different for the three ACs. However, the iodine value and CCl_4 activity were found to increase in the order AC3> AC2 > AC1, indicative of change in adsorption behaviour (Table 2). AC3 exhibited the highest ζ- potential among the three ACs in aqueous medium. The ζ-potential could not be measured in ethanolic medium as agglomeration of the AC was higher in ethanol preventing its suspension in ethanol.

The organic content in the ACs was derived from the thermogravimetric analysis (TGA) of the ACs[30]. The TGA profiles of the synthesized ACs in air showed similar thermal properties, with two step decomposition reaction (Figure 9a). The first step of mass reduction was observed in the temperature region of room temperature to 125 ºC and is well below 10 % which could be attributed to the loss of surface adsorbed moisture. This initial mass loss in the ACs may be related to the presence of oxygenated surface groups, responsible for hydrogen bonding developed between the ACs and the entrapped moisture. The onset of the second step decomposition irrespective of the ACs, started at 300°C, however the amount of residual formed was dependent on the nature of ACs[35]. The second degradation step was attributed to the degradation of the lignocellulosic structures. The TGA results indicated that the carbonization condition in the AC obtained from the coconut shell should be established at higher temperatures (400–700 °C) to obtain a carbon-rich product. Also, it should be emphasized that the low level of ashes found in ACs (Table 2), is an important property in choosing a good precursor like coconut shell for the AC production. The presence of ashes can affect the chemical characteristics and the adsorptive behaviour of AC, hence the low ash level found in the studied AC is desirable. TG studies in nitrogen atmosphere showed higher mass loss in AC1. This was indicative of the presence of an oxygen rich functional group which supports combustion in an inert atmosphere and that the

oxygen rich organic content in the ACs followed the order AC1>AC2>AC3 (Plot (a) of Figure 10). As the TGA is comparatively broad, for clear thermal degradation pattern, DTA of AC1, AC2 and AC3 in air and nitrogen atmosphere were performed (Figure 9b and Figure10b). The DTA of the ACs under aerated condition exhibited broad exothermic peak in the temperature range from 400 to 800 °C which are attributed to combustion of the organic content in the ACs. Further, DTA thermogram under nitrogen atmosphere exhibited exothermic peak centred at ~ 555°C for AC1 and AC2. The exothermic peak in presence of N_2 confirmed the presence of oxygen organic content, which may be due to lignocellulosic decomposition. The higher exothermic peak for AC1 is an indicator of higher oxygen organic content compared to the other ACs[35].

SEM was carried out to find the surface morphology of the ACs. The SEM image shows that the surface morphology of the ACs strongly depend on the treatment condition (Figure 9c, Figure 10c & 10d)[36]. The SEM micrographs of AC1 and AC2 showed pores of irregular sizes with cracks observed at the edges of carbon surface. However, the pore density was higher in AC2 as compared to AC1. Contrary to this, the SEM image of AC3 carbon showed a systematic pattern of oval pores with smooth surface structures. These SEM images clearly indicated that AC3 has more regular porous structure, which results in its higher CCl_4 and iodine values.

The Raman spectra of ACs (Figure 9d) are characterized by presence of two bands centred at 1600 cm^{-1} and 1350 cm^{-1}, generally termed as G-band and the D-band respectively[37]. The D-band induced by sp^3 electronic states is caused by the defects in the planar sp^2 graphitic structure. The G band, which is related to the graphite E_2g symmetry of the interlayer mode reflects the structural integrity of sp^2 –hybridised carbon atoms in carbon samples. In material characterization, these bands are used to estimate the extent of defects present in any carbon material. The intensity ratios of the D to the G band (I_D/I_G) irrespective of the nature of ACs remained nearly one. The result indicated that the physical activation of the ACs did not alter the ratio of defects but changed only the extent of pore formation.

The adsorption isotherm showing the volume of N_2 gas adsorbed/ desorbed with respect to the relative pressure ratio for the ACs is presented in Figure 11. The volume of the gas adsorbed on the ACs as a function of relative pressure increased exponentially and reached a plateau at relatively lower pressure of approximately 0.4, which is an indicative of a microporous structure. The N_2 adsorption/ desorption isotherms were used to calculate the

monolayer volume (ncc/g), specific surface area (m^2/g) and micro-pore volume by means of the Dubinin method[38]. The micropore volume, monolayer volume and specific surface area of AC3 were higher than that of AC2 and AC1 (Table 3).

Adsorption efficiency comparison:

Adsorption of PM567 dye in ethanol medium was determined for all the ACs. The comparative adsorption of PM567 on AC1, AC2 and AC3 and the adsorption efficiency in the order of AC1<AC2≤PAC&AC3 (Figure 12), corroborate the effect of higher porosity and specific surface area on increased dye adsorption.

Conclusions

In conclusion, a comparison of the PM567 dye removal efficiency in ethanol by γ-radiolysis and adsorption showed that adsorption by activated carbon synthesized from bio-waste was 95% efficient while it was limited to 62% by γ-radiolysis at 3.5 kGy. This low efficiency ethanol solvent by γ-radiolysis was due to geminate recombinant reactions of the dye degrading radicals formed leading to a very low radiochemical yield of 21 $nmol.J^{-1}$. The present investigation also revealed that powdered activated carbon demonstrated the highest efficiency in PM567 dye adsorption from ethanol among the examined adsorbents. To further optimize its utility in a packed bed configuration, a simple method for synthesizing granular activated carbon (AC1, AC2, and AC3) through time-dependent steam activation of coconut shell bio-waste was optimized. Notably, granular AC3 exhibited comparable adsorption efficiency (95 ± 4%) to powdered activated carbon, attributed to its higher surface area (1708 $m^2.g^{-1}$) and pore volume (0.61 $cc.g^{-1}$). This initial comparison highlights the superior performance of activated carbon in adsorption compared to radiation-induced degradation. Moving forward, the future studies will focus on understanding batch adsorption mechanism in non-aqueous effluents, and exploring the feasibility of transitioning from batch processes to a packed adsorption column configuration.

Acknowledgements:

The authors would like to express their gratitude to Dr. Archana Sharma, Director, BTDG, BARC, Shri Soumitra Kundu, Head, ATLAD, BARC and Dr. Awadhesh Kumar, Associate Director, CG, BARC for supporting this work. Dr. K. Dasgupta, G& AMD, BARC is acknowledged for the Raman spectra and surface area analysis. Dr. Sunita Kedia, L& PTD

is acknowledged for the SEM analysis. Dr. Gautam S., Head, FTD, BARC is acknowledged for permitting to use the orbital incubator shaker. Shri Sunil Dehade is acknowledged for his assistance in the experimental work. M/s. Industrial Chemicals, Gujarat, India is acknowledged for use of their facility to synthesize the activated carbons.

Figures:

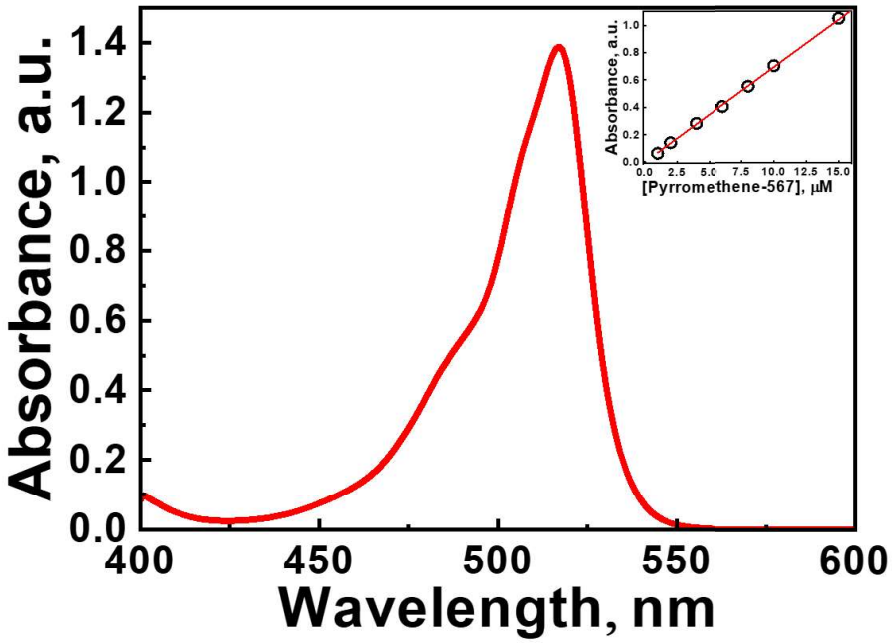

Fig. 1: Absorption spectrum of PM567 in ethanol. Inset shows the plot to estimate extinction coefficient of PM567 in ethanol

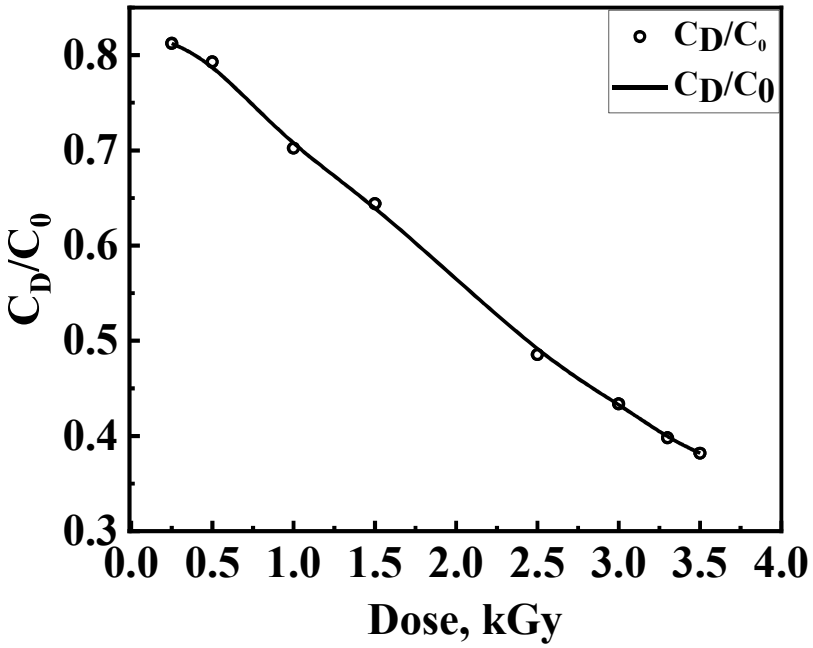

Fig. 2: PM567 dye degradation ratio (C_D/C_0) as a function of absorbed dose after gamma radiolysis in ethanol solvent

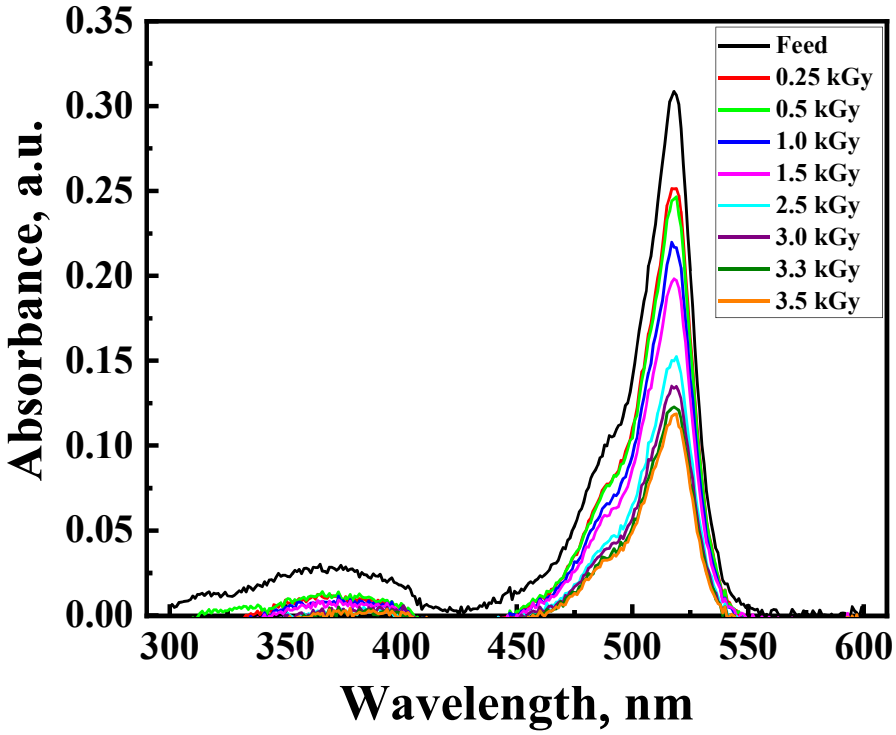

Fig. 3: Dose dependent absorbance spectra of feed and γ-radiolysed PM567 dye in ethanol

Fig. 4: PM567 feed and gamma radiolysed degraded dye at different absorbed doses (in ethanol)

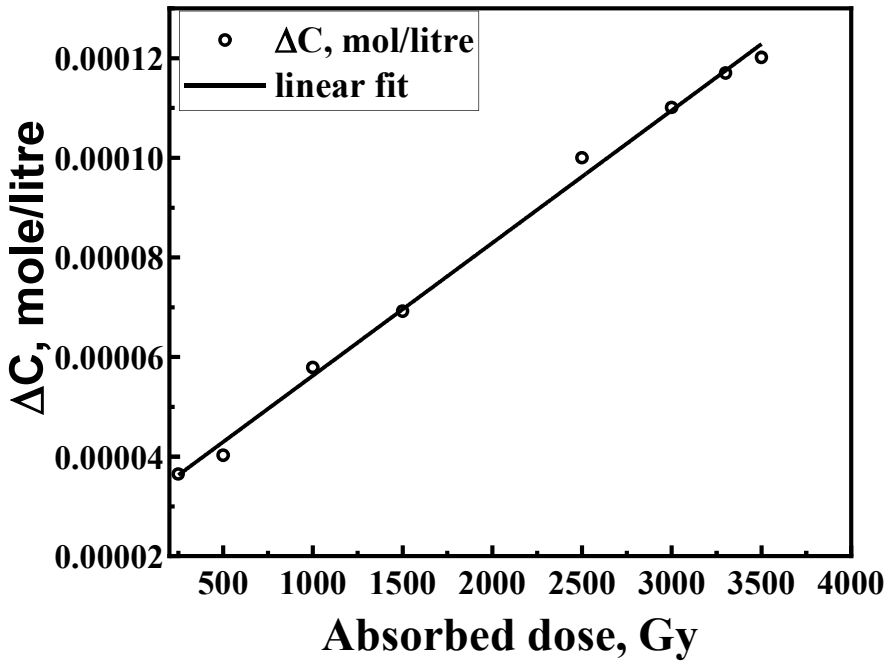

Fig. 5: G-value estimation for PM567 dye degradation by gamma radiolysis in ethanol

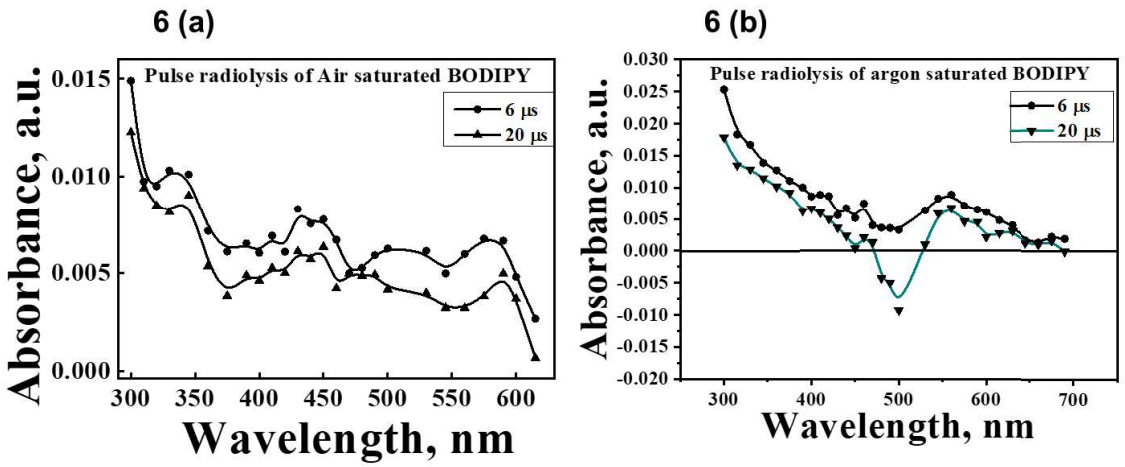

Fig. 6: Pulse radiolysis of (a) air saturated PM567, (b) Argon saturated PM567 in ethanol

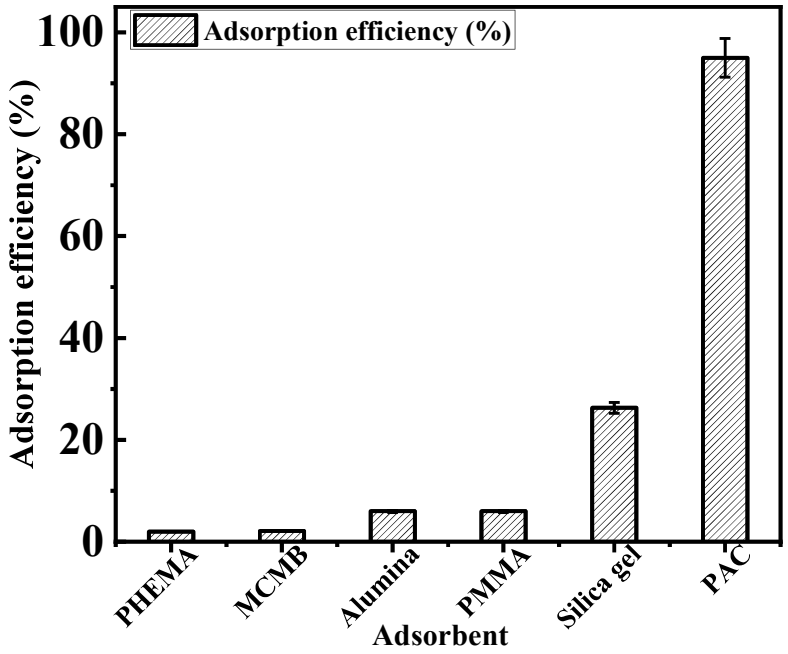

Fig. 7: Adsorption efficiency (%) for PM567 in ethanol solvent on commercial adsorbents

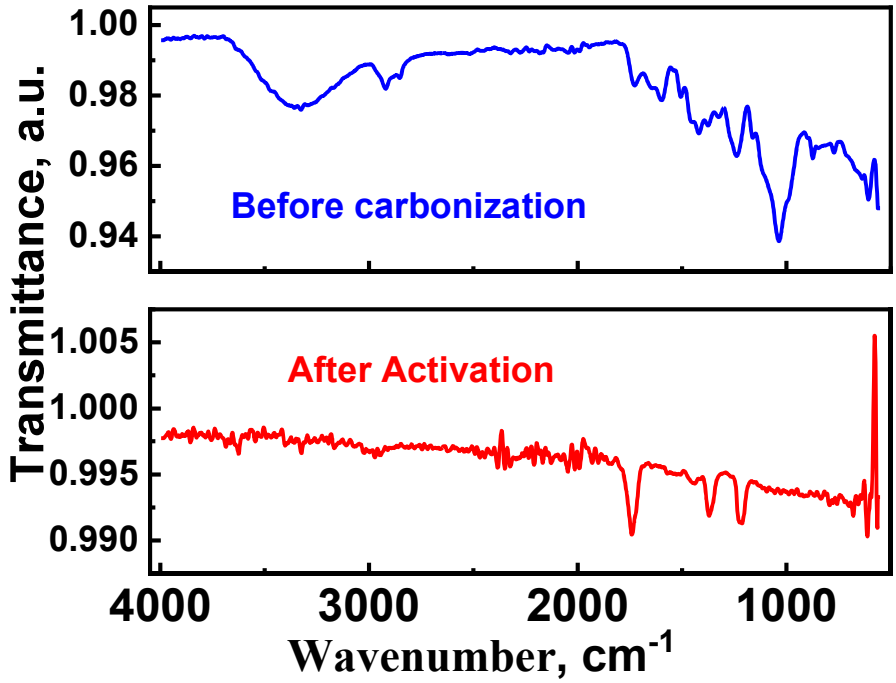

Fig. 8: FT-IR spectrum obtained from coconut shell before carbonization (blue) and after steam activation (red)

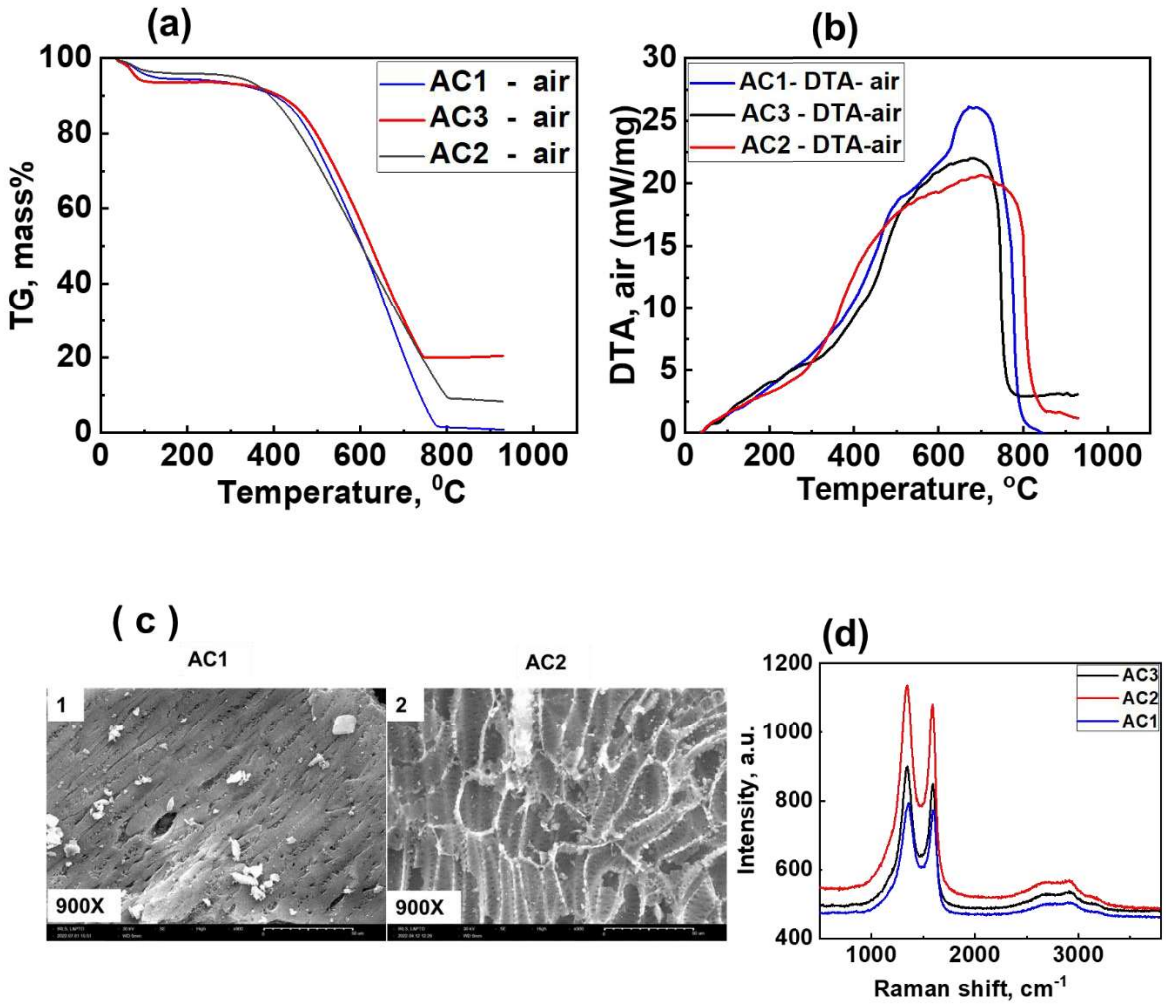

Fig. 9: (a) Thermogram of ACs in air (b) DTA of ACs in air (c) SEM of AC1 and AC2, (d) Raman spectra of ACs

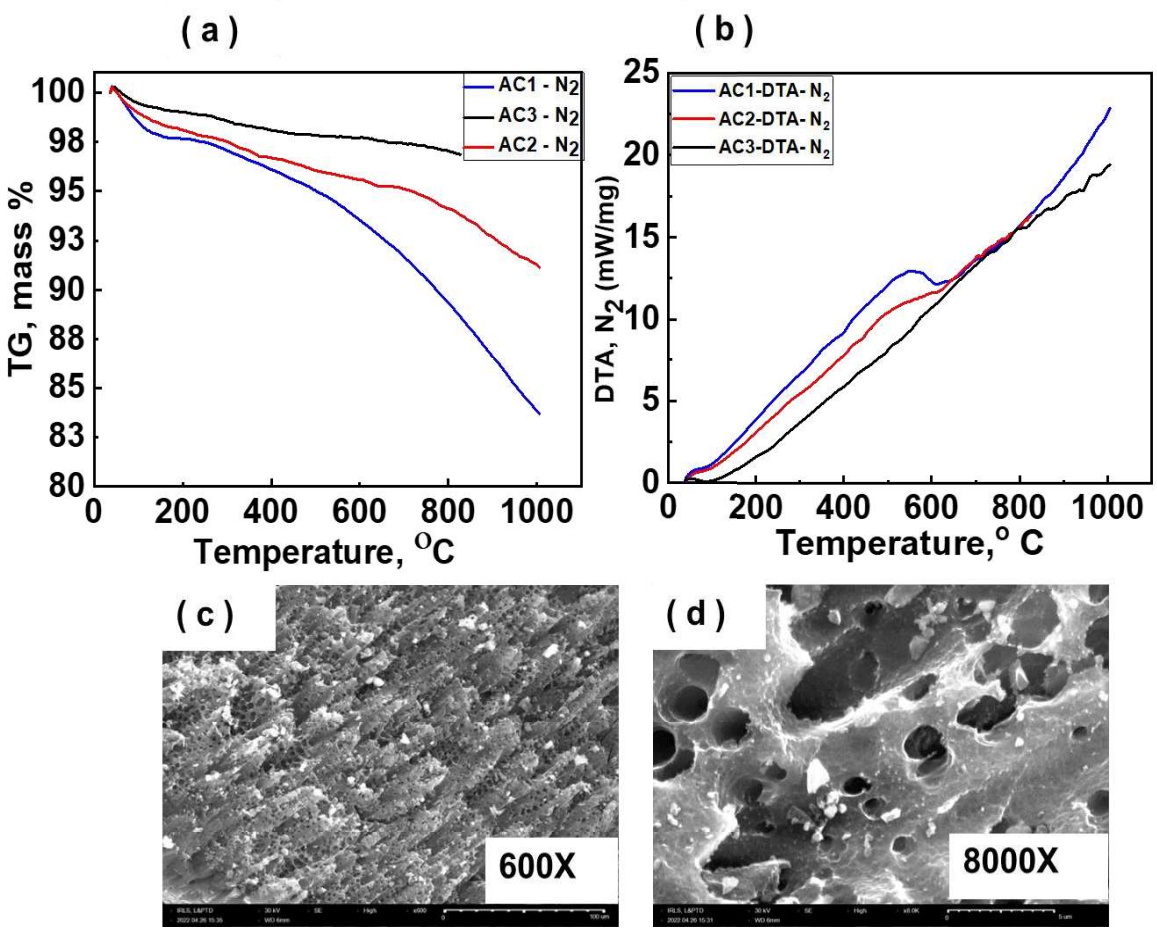

Fig. 10: Plot (a) The respective thermogram of different ACs in presence of inert condition. Plot (b) The DTA plot of the different ACs obtained on heating under N_2 condition. Plot (c) and Plot (d) are the SEM images of the AC3 at two different resolutions.

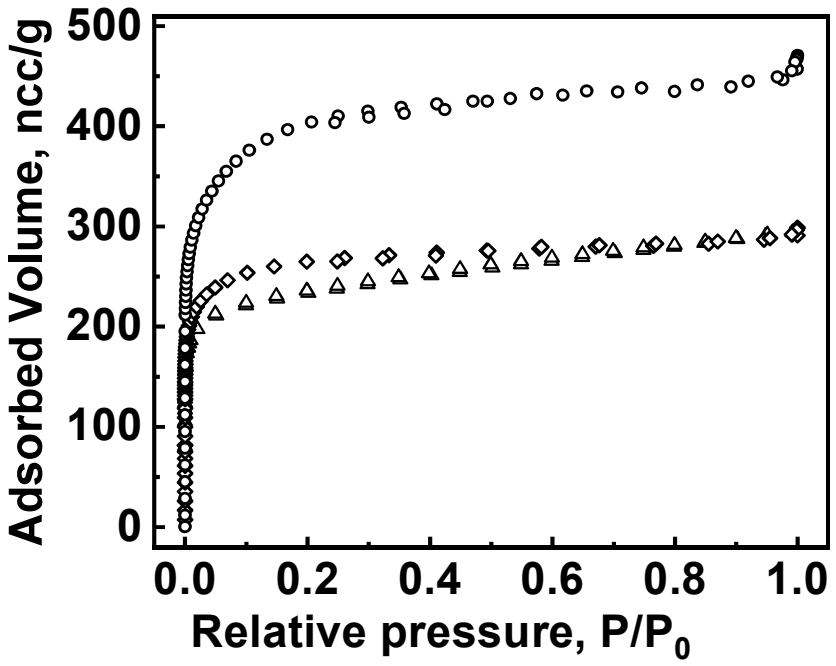

Fig. 11: Isotherm (BET) for AC1 (Δ) AC2 (◇) and AC3 (○)

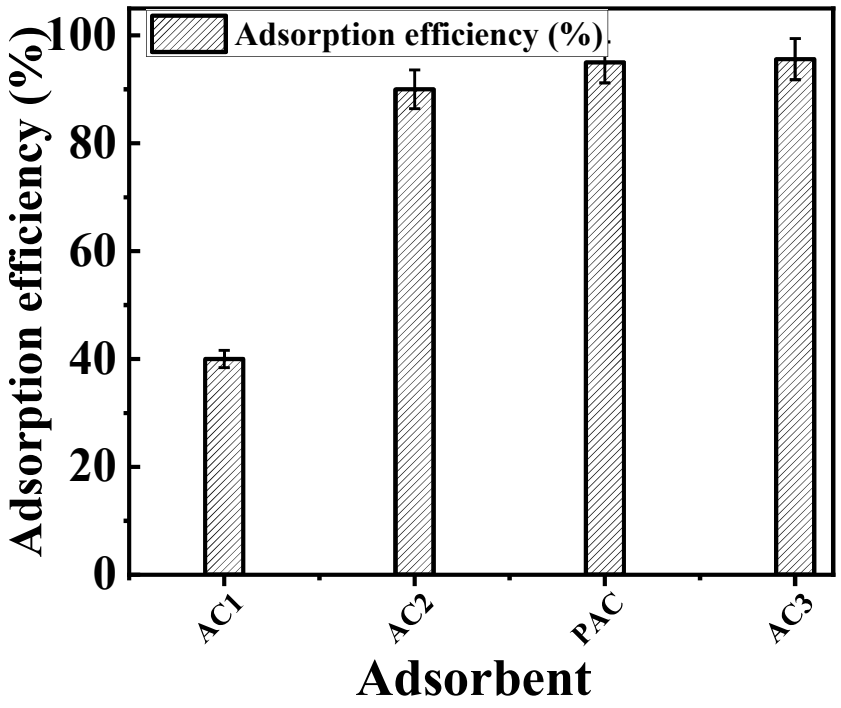

Fig. 12: Comparison of Adsorption efficiency (%) of ACs

Tables:

Table 1: Properties of PM567 dye

Molecular formula	$C_{18}H_{25}BF_2N_2$
Molecular weight	318.22
λ_{max} (nm) for UV Visible absorption	518
Molecular volume	273.373 Å^3

Table 2: Physico-chemical properties of the ACs

Parameter	AC1	AC2	AC3
Bulk density (gcm^{-3})	0.5	0.5	0.4
Moisture Content (%)	2%	2%	2%
Ash content (%)	2.9 %	2.7%	2.7%
Hardness	99.2	96.1	96.1
pH	7	7	7
Iodine number (mg/g)	1017	1245	1340
CCl_4 activity	43	53	>85
ζ - potential in water, mV	-31.4	-34.7	-38.5

Table 3: N_2 adsorption/desorption isotherm data of the ACs

Parameter	**AC1**	**AC2**	**AC3**
Monolayer volume (ncc/g)	202.3	260.1	392.4
Specific surface area (m^2/g)	880	1132	1708
μ-pore volume (cc/g)	0.27	0.40	0.61
Average pore radius (Å)	< 20	21.2	20.7
Correlation factor	0.975	0.982	0.974

References

1. Lakshmi Vellanki, Ritambhara Sharma & Ravikanth Mangalampalli, Reports Org Chem., Taylor & Francis, London, 1, 2016.
2. K K Jagtap, D K Maity, A K Ray, K Dasgupta, S K Ghosh., Pramana - J Phys. 75(5), 985, 2010.
3. V S Rawat, J Mukherjee, L M Gantayet, Prog Quantum Electronics, 43, 31, 2015.
4. S Sinha, S Sasikumar, A K Ray, Dasgupta K, Appl Phys B Lasers Opt.;78(3-4), 401, 2004.
5. Ferrero F, Periolatto M, Rovero G, Giansetti M, J Clean Prod. 19 (12), 1377, 2011.
6. A L Lotts, M L Spaeth, J I Davis, AVLIS Production Plant Waste Management Plan, UCID-20197, Lawerence Livermore National Laboratory, Oak Ridge, USA, 1984.
7. S Mondal, M K Purkait, S De, Advances in Dye Removal Technologies, Springer, Singapore, 2018.
8. J P Guin, Y K Bhardwaj, D B Naik, L Varshney., RSC Adv., 4(96), 53921, 2014.
9. F S Wahshi, M D Alqahtani, M Abdulla, T Ramachandran, F Hamed, T Thiemann, 48, 10, 2020.
10. S K Parida, S Dash, S Patel, B K Mishra, Adv Colloid Interface Sci., 121(1-3):77, 2006.
11. E P Fernandes, T S Silva, C M Carvalho, et al., J Environ Chem Eng.,9(5), 106198, 2021.
12. R S Dassanayake, S Acharya, N Abidi, Molecules. 26(15), 4697, 2021.
13. A G Rios, L C Matos, Y A Manrique, J M Loureiro, A Mendes, A F P Ferreira., Adsorption, 26(1), 75, 2020.
14. G Mezohegyi, F P Van der Zee, J Font, A Fortuny, A Fabregat, J Environ Manage. 102, 148, 2012.
15. M M Hassan, C M Carr, Chemosphere, 265, 129087, 2021.
16. R Kabir Ahmad, S Anwar Sulaiman, S Yusup, Sham Dol S, Inayat M, Aminu Umar H., Ain Shams Eng J., 13(1), 101499, 2022.
17. Standard Practice for Using the Fricke Dosimetry System, ASTM ISO/ASTME1026-15, ISO, Geneva, 2015.
18. S.N.Guha, P.N.Moorthy, K. Kishore DBN and KNR, *Chem Sci*. 99(4), 261, 1987.
19. P González-García, Renew Sustain Energy Rev., 82, 1393, 2018.
20. Indian Standard, IS 877(2), Bureau Indian Standards, New Delhi, 1990.

21. Indian Standard, IS 2752, Bureau of Indian Standards, New Delhi, 1995.
22. D Jore, N Champion, N Kaouadji, J P Jay-Gerin, & C Ferradini, International Journal of Radiation Applications and Instrumentation. Part C. Radiation Physics and Chemistry 32(3), 443, 1988.
23. R Changotra, J P Guin, S A Khader, A Dhir, J Environ Chem Eng., 8(5), 104423, 2020
24. S.N.Guha, P.N.Moorthy, K. Kishore DBN and KNR, Chem Sci. 99(4), 261, 1987.
25. Shigeki Hattori, Kei Ohkubo, Yasuteru Urano, Hisato Sunahara, Tetsuo Nagano, Yuji Wada, Nikolai V. Tkachenko, Helge Lemmetyinen, and Shunichi Fukuzumi, J Phys Chem B., 109(32), 15368, 2005.
26. Y Qi, T Geib, A M Huynh, G Jung, DA Volmer, Rapid Commun Mass Spectrom., 29(9), 885, 2015.
27. Victoria J. Richards, Alexandra L. Gower, Jasper E. H. B. Smith, E. Stephen Davies, Dorothe´e Lahaye, Anna G. Slater (ne´e Phillips), William Lewis, Alexander J. Blake, Neil R. Champness and Deborah L. Kays, Chem Commun.; 48(12):1751, 2012.
28. M T Yagub, T K Sen, S Afroze, H M Ang., A review. Adv Colloid Interface Sci., 209, 172, 2014.
29. H Patel, Int J Environ Sci Technol., 19(10), 10409, 2022.
30. Q Wang, J Sarkar, Int J Energy Prod Manag. 3(1), 34, 2018.
31. R Krishnan, L Hauchhum, R Gupta, S Pattanayak., 2nd International Conference on Energy, Power and Environment : Theme: Towards Smart Technology : ICEPE-2018, NIT, Meghalaya, PP 1, June, 2018.
32. A Rehman, M Park, S J Park., Coatings.;9(2), 1, 2019.
33. S Zhao, L Chen, Biomass Convers Biorefinery. 12(9), 3943, 2022.
34. H Madzaki, Wawab Karimghani, Nurzalikharebitanim, Azilbaharialias., Procedia Eng., 148, 718, 2016.
35. A Bazan, P Nowicki, P Półrolniczak, R Pietrzak, J Therm Anal Calorim., 25(3), 1199, 2016.
36. Tsai WT, Jiang TJ., Biomass Convers Biorefinery, 8(3), 711, 2018.
37. N M Keppetipola, M Dissanayake, P Dissanayake, et al., RSC Adv., 11(5), 2854, 2021.
38. C Bläker, J Muthmann, C Pasel, D Bathen, Chem BioEng Rev., 6(4), 119, 2019.